Pisco-Med Publishing

Synthesis, Characterisation and Electrochemical Studies of Co^{2+} Doped $GdAlO_3$ for Sensor Applications

P.K. Jisha[1], Ramachandra Naik[1], S.C. Prashantha[2], H. Nagabhushana[3], H. P Nagaswarupa[1], C.R Ravikumar[1]

[1] Department of Physics, New Horizon College of Engineering, Bangalore-560103, India

[2] Research Center, Department of Science, East West Institute of Technology ,VTU, Bangaluru-560091, India

[3] Rao Center for Advanced materials, Tumkur University, Tumkur-572103, India

Abstract: The structural and electrochemical properties of cobalt (Co^{2+}) doped GdAlO3 nanoparticles have been investigated. Structure analysis was carried out using X-ray diffraction (XRD) and Transmission electron microscope technique (TEM). The electrochemical properties of the GdAlO3:Co^{2+} (3 mol %) was measured using cyclic voltammetry (CV) and electrochemical impedance spectroscopy (EIS) measurements using 1 M KOH electrolyte and 1 M KOH electrolyte with 2 ml of Paracetamol. The cyclic voltammetry measurements indicate that the reversibility of the electrode reaction increases while adding 2 ml of Paracetamol. Whereas, the EIS measurements reveal that a reduction in the charge transfer resistance increases capacitance of the GdAlO3:Co^{2+} electrode.

Keywords: Combustion; Fourier transform infrared; Diffuse Reflectance; Cyclic voltammetry; Electrochemical impedance spectroscopy

1. Introduction

In 21st century, energy is a fundamental worldwide issue for the human society .Energy we needed is provided by fossil fules.But it is not renewable and also it emits pollutants while burning which degrade the environment and green-house gases lead to global warming problem[1,2]. Such frameworks require the advantages of compactness and en-ergy effectiveness while being environmental friendly[3]. The technology and systems of an external thermal inter-face or that of an external electrical interface embrace by Energy conversion and storage systems[4].Based on amount of energy and power available for the load they are categorised into groups which includes batteries, fuel cells, capacitors and supercapacitor[5,6].

Among various energy storage systems electrochemical capacitors also known as super capacitor can provide high power capabilities, excellent reversibility and long cycle life[7,8] and it bridges the energy gap between capacitors (high power output) and fuel cells/batteries (high energy storage)[9,10]. Many researches focussed for the improve-ment for the better performance of supercapacitors by using carbonaceous compound, metal oxides, conducting polymers and the associated hybrids/ composites as promising electrode materials[11-13].

Complex oxides like ABO3 are a class of chemically and thermally stable materials, which are suitable for a wide range of applications, such as magnetic, optical, ceramics, and catalysis[14]. Among these Rare earth ortho aluminates REAlO3 materials are better candidates, because of their excellent properties, like high thermal stability, high me-chanical resistance, hydrophobicity, and low surface acidity[15]. In previous studies it is found that gadolinium aluminate (GdAlO3) is a potential host system for materials with oxygen ion conductivity[16].

In order to study the effect of cation dopant on the structure, Cyclic Voltammetry and ac impedence of perovskite GdAlO3, In this paper GdAlO3:Co2+ prepaired by solution combustion method[17] and studied its characteristics, Diffuse reflectance spectra (DRS) and Fourier Transform Infrared (FTIR), in addition to that comparative study of CV, EIS[18] in presence and absence of Paracetamol in 1 M KOH electrolyte.

doi: 10.18282/pef.v7i1.90

2. Experimental

2.1 Preparation of sample

$GdAlO_3:CO^{2+}$ (1-7 mol %) synthesised using the solution combustion method by using stoichiometric quantities of gadolinium nitrate [Gd $(NO_3)_3$], aluminium nitrate (Al $(NO3)_2$, cobalt nitrate CO $(NO_3)_2$, laboratory prepared Oxalyl dihydrazide (ODH:$C_2H_6N_4O_2$) fuel were dissolved in doubled distilled water. A homogeneous solution obtained after stirring 15min. The resultant solution was placed in a furnace pre heated at 400oC for, until surplus free water evaporated and natural ignition occurred ensuing in a fine powder product obtained after grinding. Finally, the as prepared powders were calcined at 1000 ℃ for 3 h. The resulting $GdAlO_3$: CO^{2+}powder were cooled down to room temperature and mixed well by using a pestle and mortar[17].

2.2 Preparation of the modified electrode

The sample, graphite powder and silicone oil ratio was 15:70:15 % by weight and were mixed in an agate mortar for about 40 min. the carbon paste was packed in to the of homemade carbon paste electrode and then smoothened on a tissue paper till the surface become uniform.

2.3 Instrumentation

The crystalline nature of the powder sample is characterized by PXRD using X-ray diffractometer (Shimadzu) (operat-ing at 50 kV and 20mA by means of CuK((1.541Å) radiation with a nickel filter at a scan rate of 2omin-1). Trans-mission Electron Microscopy (TEM) analysis is performed on a JEOL, JEM-2100 (accelerating voltage up to 200 kV, LaB6 filament) . diffuse reflectance spectra (DRS) were recorded using Shimadzu UV–visible spectrophotom-eter model 2600. Fourier transform infrared (FTIR) studies of the samples are performed with a Perkin Elmer FTIR spectrophotometer (Spectrum-1000). For cyclic voltammetric tests, the measurement was performed on a CHI604E potentiostat with a trielectrode system, consisting of nickel hydroxide electrode, platinum wire and Ag/AgCl as working, counter and reference electrodes respectively and the electrolyte being a 1 M KOH solution. The potential range was −0.2 V to 0.6 V (vs. Ag/AgCl electrode) and the scanning rate was 10 mV/s, 20 mV/s, 30 mV/s, 40 mV/s and 50 mV/s. In addition, with AC amplitude of 5 mV and frequency range of 1 Hz to 1 MHz, EIS measurements were also carried carried out.

3. Results and discussion

3.1 PXRD AnalysiS

The XRD pattern of 1000 ℃ calcinated combustion product indicate that fully crystallized single phase $GdAlO_3:CO^{2+}$ were obtained as shown in the **Figure 1**.

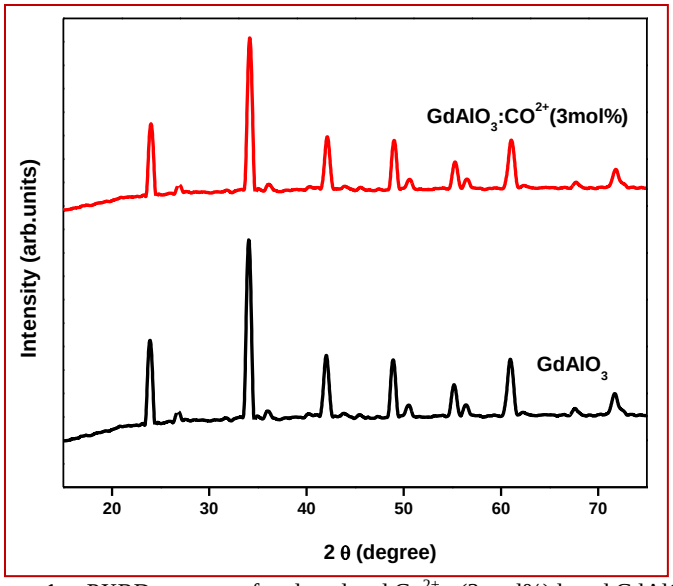

Figure 1. PXRD patterns of undoped and Co^{2+} (3 mol%)doped $GdAlO_3$.

All the peaks in the XRD pattern are in good agreement with JCPDS File No. 46-0395[19], demonstrating the formation of $GdAlO_3$ phase with orthorhombic perovskite structure indicates that all the dopants(CO^{2+}) have successfully been incorporated into the host matrix($GdAlO_3$). The effect of crystallinity on the crystallite size of the samples crystallite size (D) was estimated from the line broadening in X-ray powder using Scherrer's formula[20].

$$D = \frac{K\lambda}{\beta\cos\theta} - - - - - - - (1)$$

where, 'K'; constant, λ; wavelength of X-rays, and 'β';

FWHM was found to be in the range 15-25 nm.

3.2 Transmission electron microscope (TEM)

The morphology, structure and particle size of the prepared $GdAlO_3$:CO^{2+}sample characterize by TEM image. Selected Area Electron Diffraction (SAED) pattern and particle size distribution as shown in **Figure 2a** and **Figure 2b**. The ring nature of the electron diffraction pattern is an indicator of the polycrystalline nature of the crystallites. The crystal structure and particle size 20nm obtained by the analysis of TEM micrograph which was in good agreement to those obtained by Scherrer's formula.

3.3 Fourier transformation infrared spectroscope (FTIR) of $GdAlO_3$: Co^{2+}

Figure 3 shows the FTIR spectra of solid state synthesized $GdAlO_3$:Co^{2+} (3 mol %). A strong band between 400 and 800 cm^{-1} are the characteristic of Metal-Oxygen stretching vibrations and O-M-O bending vibrations for the perovskite structured compounds[21]. The A strong absorption peak at 683 cm^{-1} corresponds to Gd/M-O vibrational modes. The band at 457cm^{-1} attributed to the CO-O stretching[22,23]. A narrowband at 1594 cm^{-1} assigned to the stretching and bending modes of adsorbed water.

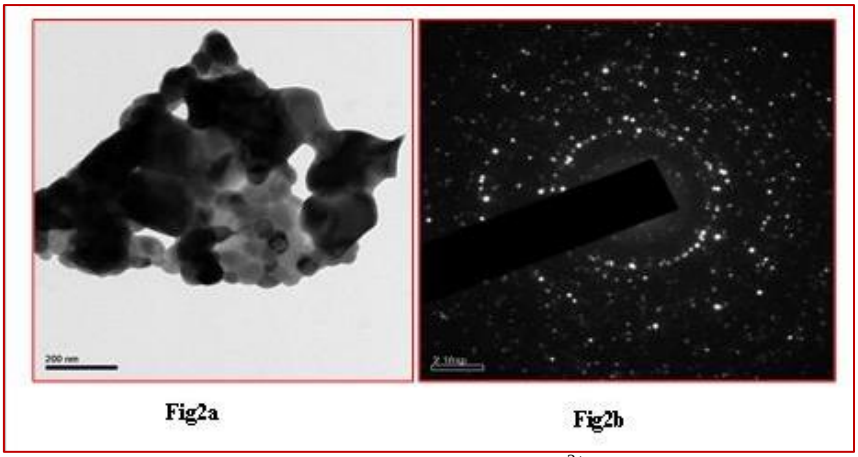

Figure 2. a) TEM and **b**) SAED images Co^{2+} doped $GdAlO_3$.

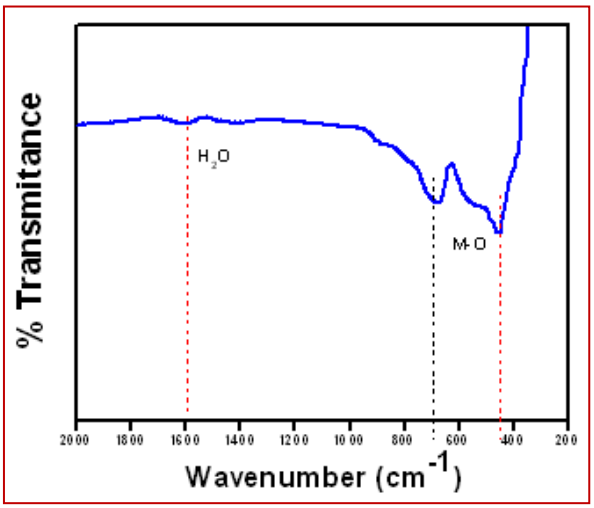

Figure 3. FT-IR spectra Co^{2+} of doped $GdAlO_3$.

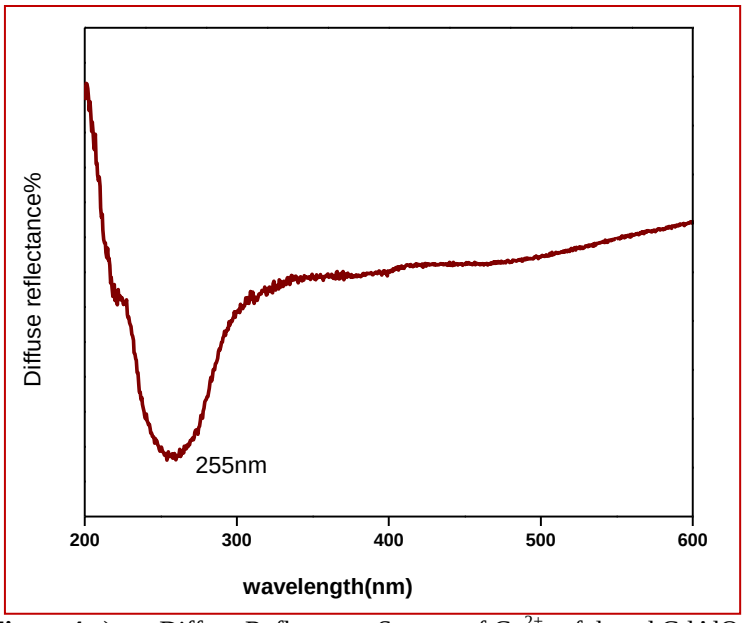

Figure 4 a). Diffuse Reflectance Spectra of Co^{2+} of doped $GdAlO_3$.

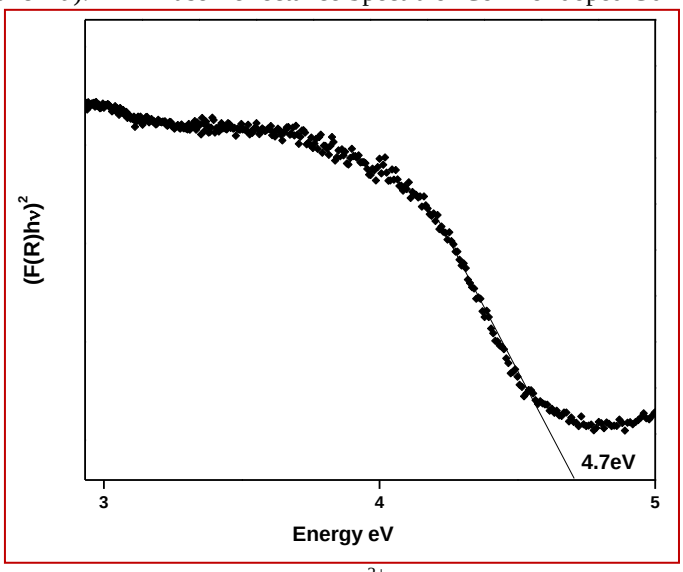

b). Band gap values of Co^{2+} of doped $GdAlO_3$.

3.4 Optical studies

In the optical studies, diffuse reflectance spectra were measured and band gap calculated from diffuse reflectance spectra. The diffuse reflectance spectra of the doped sample were measured against reference standard spectra. A sharp band at 255 nm was observed for the samples as shown in **Figure 4a**.

This corresponds that light having this particular wavelength was absorbed. Band gap calculated based on Kubelka Munk[24,25] theory for the Co^{2+} (3 mol%) doped $GdAlO_3$ nanophosphor. The relation between the diffuse reflectance of the sample (R), absorption coefficient (K) and scattering coefficient (S) is given by the Kubelka-Munk function F(R).

$$F(R) = \frac{(1-R)^2}{2R} = \frac{K}{S} - - - - (2)$$

Tauc relation for direct band gap is the relation between band gap (Eg) and linear absorption coefficient (α) of a material, Tauc relation is given by

$$\alpha h\nu = C1(h\nu - Eg)^{1/2} - - - - - - - - (3)$$

Considering the scattering coefficient 'S' as constant with respect to wavelength, and combining Eqs. (3) and (4), result in the following expression,

$$[F(R\infty)h\nu]^2 = C2(h\nu - Eg) - - - - - - - - (4)$$

From the plot of $(F(R)h\nu)^2$ versus hν, the value of E_g was obtained by extrapolating the linear fitted regions to $(F(R_\infty)h\nu)^2=0$. The curve of **Figure 4b** exhibits nonlinear and linear portions, which is the characteristic of direct allowed transition. The nonlinear portion

corresponds to a residual absorption involving impurity states and linear portion characterizes the fundamental absorption. The band gap s found to be which is equal to 4.7 eV.

3.5 Cyclic voltammetry (CV)

CV is an electrochemical technique which measures the current that develops in an electrochemical cell under conditions where voltage is in excess of that predicted by the Nernst equation. CV is performed by cycling the potential of a working electrode, and measuring the resulting current.

Cyclic voltammetry is a commonly used method of measuring the reduction potential of a species in solution. The species may be a coordination complex or a redox-active organic compound, for example. Cyclic voltammetry provides additional data that can be interpreted to make conclusions about the reduction/oxidation reaction and the stability of the species resulting from the electron transfer[26,27].

In cyclic voltammetry, rather than measuring the voltage produced by a reaction as we discussed before, a voltage is instead applied to the solution. The voltage is changed over time and current through a circuit is monitored. When the voltage reaches a point at which a reduction/oxidation is induced, current begins to flow. A cyclic voltammogram is a plot of current versus applied voltage.The potential of the working electrode is measured against a reference electrode which maintains a constant potential, and the resulting applied potential produces an excitation signal as shown.

Figure 5a shows CV recorded in 1 M KOH electrolyte for Cobalt doped $GdAlO_3$ in 1M KOH electrolyte at five different scan rates (10, 20, 30, 40 and 50 mVs^{-1})[28]. CVs provide valuable information on reduction oxidation (charge-discharge) behavior of electrodes. Here, the capacitance was mainly based on the redox reaction because the shapes of the CVs were distinguished from the shape of the electric double-layer capacitance, which is normally close to an ideal rectangle[29,30]. As the scan rate was increased, the current response, which is a measure of the capacitance, also increased. The relatively higher current density for the Cobalt doped $GdAlO_3$ indicates good rate capability for battery and supercapacitor applications. Fig. 5b shows CV of Cobalt doped $GdAlO_3$ in 1 M KOH electrolyte with 2 ml of Paracetamol, this results shows the prepared electrode material is used for sensor applications.

3.6 AC impedence

With AC amplitude of 5 mV and frequency range of 1Hz to 1 MHz, EIS measurements were also carried out. **Figure 8** represents the electrochemical impedance spectra of Cobalt doped $GdAlO_3$ .The spectra shows a depressed two-dimensional figure ensuring charge transfer resistance within the high-frequency region, and a slope associated with Warburg resistance within the low-frequency region[31,32]. The charge transfer resistance (R_{ct}) and double layer capacitance (C) values obtained from fitting the equivalent circuit **Figure 6a** for impedance spectra, as given in **Table 1**$GdAlO_3$ in 1M KOH electrolyte.

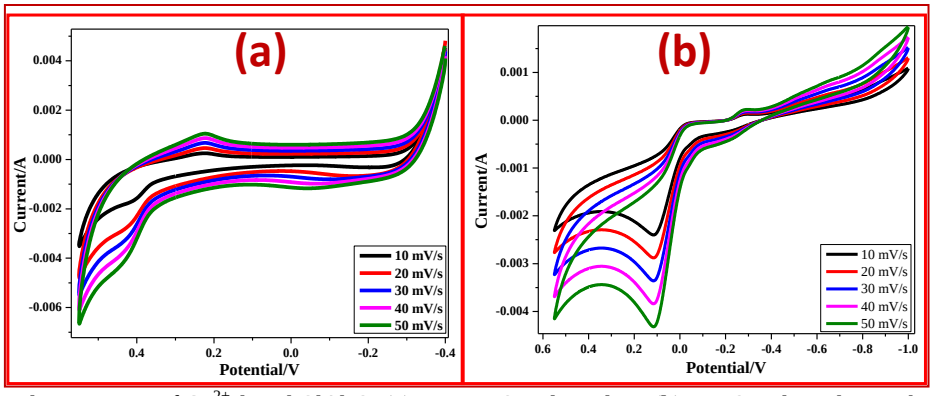

Figure 5. Cyclic voltammogram of Co^{2+} doped $GlAl_2O_3$ (**a**) in 1M KOH electrolyte. (**b**) in KOH electrolyte with 2 ml of Paracetamol.

Name of the electrode	Charge-transfer resistance (R_{Ct})	Capacitance of double layer (C_{dl})
Cobalt doped $GlAl_2O_3$ in 1M KOH electrolyte	0.0336	5.517×10^{-4}
Cobalt doped $GlAl_2O_3$ in 1M KOH electrolyte with Paracetamol	27.38	6.638×10^{-8}

Table 1. Capacitance and resistance of different electrodes

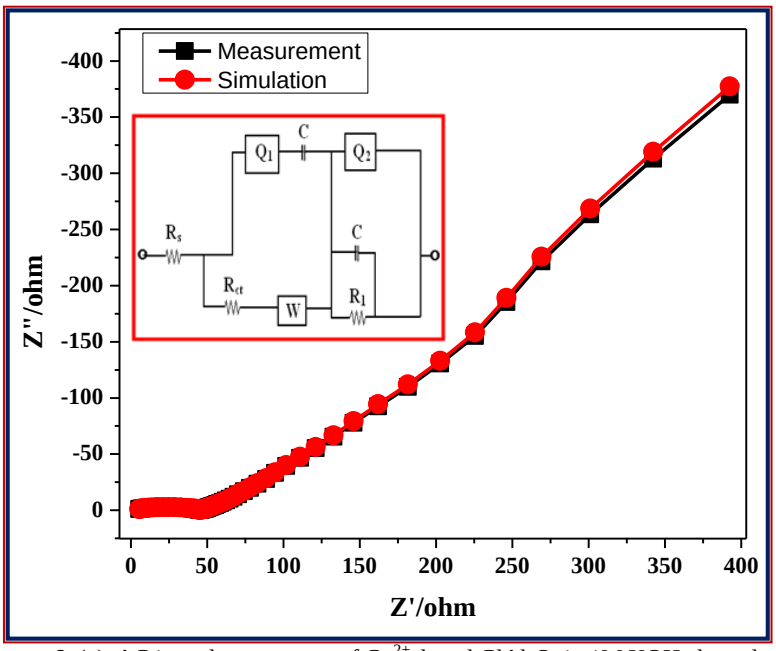

Figure 6. (**a**). AC impedance spectra of Co^{2+} doped $GlAl_2O_3$ in 1M KOH electrolyte.

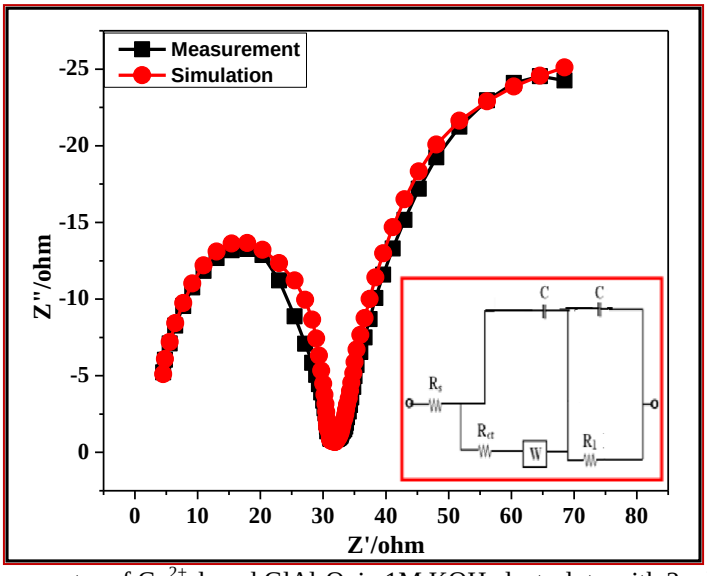

(**b**). AC impedance spectra of Co^{2+} doped $GlAl_2O_3$ in 1M KOH electrolyte with 2 ml of Paracetamol.

The **Figure 6a** represents Warburg part that is within the low-frequency region of impedance spectra; Q_1 represents the constant section that is parallel to the charge-transfer resistance (R_{ct}) and also the low frequency capacitance (Q_2), and is additionally parallel to the outflow resistance (R_l). In general, for a plate-like electrode, the Warburg slope is proportional to $1/CD^{1/2}$ and is about 45^0 wherever C is the concentration of diffusive species and D is the hydrogen diffusion co-efficient. This model is satisfactory for a straight forward reaction on plate-like electrodes however, for a lot of difficult reactions and porous electrodes; this is not adequate. Porous electrodes have a more complicated behaviour[33,34]. The Warburg slope of a porous electrode is between 22.5^0 and 45^0, based on characteristics of an electrode with semi-infinite pores. It is seen from **Figure 6b** that the behavior of conductor C is comparable to a plate-like electrode. The charge transfer resistance (R_{ct}) and double layer capacitance (C) values measures the two-dimensional figure at high frequencies as observed in the resistance plot. From these plots, it is clear that the charge transfer resistance is low in the electrode with $GdAlO_3:CO^{2+}$additive, followed by a rise in the capacitance of the electrode.

4. Conclusion

Cobalt doped $GdAlO_3$ compositions were prepared by solution combustion method. The structure were analysed by PXRD and TEM. The CV studies clearly indicate that Paracetamol additive were successful in increasing the reversibility by reducing the E_O-E_R value of the electrode reaction. The R_{Ct} and double layer capacitance of the electrodes were recognized by fitting the equivalent circuit for EIS spectrum. Paracetamol additive enhances the performance of the positive electrode by reducing the resistance of the $GdAlO_3:Co^{2+}$electrode. As a future perspective, we believe that $GdAlO_3:Co^{2+}$ composite material could be a promising electrode material for the fabrication of various sensors, super capacitors and solar cells.

Acknowledgements

The authors RN and SCP thanks to VGST, Govt. of Karnataka, India, (VGST/K-FIST-L1/2016-17/GRD-360) for sanctioning the research project.

References

1. J.B.Goodenough,Y.Kim, Chem. Mater. 22 (2010) 587.
2. H. Li, Z. Wang, L. Chen, X. Huang, Adv. Mater. 21 (2009) 4593.
3. L Dong, R.R.S. Gari, Z. Li, M.M. Craig, S. Hou, Carbon 48 (2010) 781–787.
4. J. Baker, Energy Policy 36 (2008) 4368–4373.
5. T. Christen, M.W. Carlen, Theory of Ragone plots, J. Power Sources 91 (2000) 210–216.
6. G. Wang, L. Zhang, J. Zhang, Chem. Soc. Rev. 41 (2012) 797–828.
7. Y. Zhang, Y. Gui, X. Wu, H. Feng, A. Zhang, L. Wang, *et al.*, Int. J. Hydrog. Energy 34 (2009) 2467–2470.
8. L. Qu, Y.J.B. Baek, L. Dai, ACS Nano 4 (2010) 1321.
9. G. Wang, L. Zhang, J. Zhang, Chem. Soc. Rev. 41 (2012) 797–828.
10. S. Bose, T. Kuila, A.K. Mishra, R. Rajasekar, N.H. Kim, J.H. Lee, J. Mater. Chem. 22 (2012) 767.
11. L. Huang, G. Guo, Y. Liu, Q. Chang, Y. Xie, J. Disp. Technol. 8 (2012) 373–376.
12. Z.-S. Wu, G. Zhou, L.-C. Yin, W. Ren, F. Li, H.-M. Cheng, Nano Energy 1 (2012) 107–131
13. Ejikeme Raphael Ezeigwe, Michelle T.T. Tan, Poi Sim Khiew, Chiu Wee Siong, Ceramics International 41 (2015) 715–724
14. X. Duan, M. Pan, F. Yu, D. Yuan, J. Alloys Compd. 509 (2011) 1079–1083.
15. D. Dhak, P. Pramanik, J. Am. Ceram. Soc. 89 (2006)1014-1021.
16. Amit Sinha , B.P. Sharma, P. Gopalan , Journal of Alloys and Compounds 536 (2012) 204–209 .
17. S.C. Prashantha, B.N. Lakshminarasappa, Fouran Singh. Curr. Appl. Phys. 11 (2011) 1273–1277.
18. Zimmerman AH,Effa, PK, J Electrochem Soc .131(1984)709
19. Wang P., Shanghai inst. of Ceramics, Chinese Academy of science, Shanghai, china, ICCD grant-in-Aid,(1994).
20. P. Klug, L.E. Alexander, X-ray Diffraction Procedure, Wiley, New York, 1954.
21. L. Shen, C. Hu, Y. Sakka, Q. Huang, , J. Phys. D Appl. Phys. 45 (2012) 215302.
22. Meza Octavio, Villabona-E. G.,Torres L. A, Desirena H., Rodr ́guez-Lopez J. L.,and Perez E., J. Phys.chem118(2014)1390-1396.
23. K. Djebaili, Z. Mekhalif, A. Boumaza, A.X.P.S.

Djelloul,, J. Spectrosc. 2015 (2015). 868109.
24. J.H. Ryu, B.G. Choi, J.W. Yoon, K.B. Shim, K. Machi, K. Hamada, J. Lumin. 124 (2007) 67-70.
25. A.E. Morales, E.S. Mora, U. Pal, Rev. Mex. Fis. S53 (5) (2007) 18-22.
26. P. Baraldi, G. Davolio, An electrochemical and spectral study of the nickel oxide electrode, Mater. Chem. Phys. 21 (1989) 143.
27. P.V. Kamath, G.N. Subbanna, Electroless nickel hydroxide: synthesis and characterization, J. Appl. Electrochem. 22 (1992) 478–482.
28. X. Cao, J. Wei, Y. Luo, Z. Zhou, Y. Zhang, Spherical nickel hydroxide composite electrode, Int. J. Hydrogen Energy 25 (2000) 643–647.
29. I. Krejci, P. Vanysek, Effect of zinc and iron ions on the electrochemistry of nickel oxide electrode: slow cyclic voltammetry, J. Power Sources 47 (1994) 79–88.
30. C.R. Ravi kumar, P. Kotteeswaran, V. Bheema Raju, A. Murugan, M.S. Santosh, H.P. Nagaswarupa, S.C. Prashantha, M.R. Anil Kumar, M.S. Shivakumar, Journal of Energy Storage 9 (2017) 12–24
31. P.R. Bueno, C. Gabrielli, H. Perrot, Electrochim. Acta 53 (2008) 5533–5539.
32. P.M.S. Monk, R.J. Mortimer, D.R. Rosseinsky, New York, 2007, pp. 312 (chapter 10).
33. M. Yen Ho, P. Sim Khiew, D. Isa, Funct. Mater. Lett. 7 (2014) 1440012.
34. M.R. Sarpoushi, M. Nasibi, M.A. Golozar, M.R. Shishesaz, M.R. Borhani, S. Noroozi, Mater. Sci. Semicond. Process. 26 (2014) 374–378.